Primary motor and sensory cortical areas communicate via spatiotemporally coordinated networks at multiple frequencies

Fritzie I. Arce-McShane[a,1], Callum F. Ross[a], Kazutaka Takahashi[a], Barry J. Sessle[b], and Nicholas G. Hatsopoulos[a,c,d,1]

[a]Department of Organismal Biology and Anatomy, University of Chicago, Chicago, IL 60637; [b]Faculty of Dentistry, University of Toronto, Toronto, ON M5G 1G6, Canada; [c]Committee on Computational Neuroscience, University of Chicago, Chicago, IL 60637; and [d]Committee on Neurobiology, University of Chicago, Chicago, IL 60637

Edited by Nancy Kopell, Boston University, Boston, MA, and approved March 9, 2016 (received for review January 22, 2016)

Skilled movements rely on sensory information to shape optimal motor responses, for which the sensory and motor cortical areas are critical. How these areas interact to mediate sensorimotor integration is largely unknown. Here, we measure intercortical coherence between the orofacial motor (MIo) and somatosensory (SIo) areas of cortex as monkeys learn to generate tongue-protrusive force. We report that coherence between MIo and SIo is reciprocal and that neuroplastic changes in coherence gradually emerge over a few days. These functional networks of coherent spiking and local field potentials exhibit frequency-specific spatiotemporal properties. During force generation, theta coherence (2–6 Hz) is prominent and exhibited by numerous paired signals; before or after force generation, coherence is evident in alpha (6–13 Hz), beta (15–30 Hz), and gamma (30–50 Hz) bands, but the functional networks are smaller and weaker. Unlike coherence in the higher frequency bands, the distribution of the phase at peak theta coherence is bimodal with peaks near 0° and ±180°, suggesting that communication between somatosensory and motor areas is coordinated temporally by the phase of theta coherence. Time-sensitive sensorimotor integration and plasticity may rely on coherence of local and large-scale functional networks for cortical processes to operate at multiple temporal and spatial scales.

motor cortex | somatosensory cortex | coherence | learning | orofacial cortex

Synchrony between cortical areas has been implicated in neuronal communication and plasticity (1–4). Sensorimotor integration and formation of motor memories during learning are examples wherein effective communication between sensory and motor areas of the cerebral cortex is critical. However, very few studies have investigated coherence between the somatosensory and motor pathways in primates (5–7). These past studies have been confined to upper limb tasks, and none of them looked at changes in coherence during learning. Here, we investigated the synchronous activity between the orofacial primary motor (MIo) and somatosensory (SIo) cortical areas that play important roles in the control of orofacial behaviors (8–10). Sensorimotor control of oral behaviors is complex, involving the integration of afferent information for moving the tongue and facial muscles. Anatomical connections between MIo and SIo are dense and both areas have bilateral orofacial representations and project to brainstem cranial nerve motor nuclei containing the motoneurons projecting to jaw, facial, and tongue muscles (11, 12). These connections provide a substrate for interareal communication between MIo and SIo for the control and learning of orofacial behaviors. To investigate cortico-cortical interactions between these areas, we measured coherence of spiking and local field potentials (LFPs) recorded simultaneously from MIo and SIo of the left hemisphere as monkeys learned a simple and controlled tongue protrusion task. Several studies using this behavioral paradigm have reported neuroplasticity and modulation of neuronal activity related to tongue protrusion separately in MIo and SIo (13–17). Here, we show that interactions between MIo and SIo involve coherent networks at multiple frequencies. Cortical processes may make use of the dynamics of oscillatory rhythms and coherence phase to coordinate the activation of sensorimotor networks at multiple spatial and temporal scales.

Results

We trained two naïve monkeys to protrude the tongue onto a force transducer and apply isometric force at the level cued by target positions shown on a video screen (Fig. 1*A*). The monkeys learned to associate the target position with the required tongue-protrusive force after a few hundred trials, but proficient task performance was achieved after 8–12 training days (Fig. 1 *B* and *C*). To investigate the emergence of interactions between MIo and SIo as monkeys learned to associate sensory information with motor response, we evaluated the coherence between the spiking of neurons recorded in MIo and SIo (MS in Fig. 2*A*) and the coherence between the spiking of MIo or SIo neurons with LFPs in SIo or MIo, respectively (MSf and SMf in Fig. 2*A*) These measures of coherence are presumed to represent the correlation of the outputs from both areas (MS) and the correlation of the outputs from one area with the inputs in the other (MSf and SMf). For each of the 5 sampled training days, D1–D5, we estimated coherence by using a 0.5-s sliding window with 0.01-s steps to show a time-resolved coherence profile in the theta (2–6 Hz), alpha (6–13 Hz), beta (15–30 Hz), and gamma (30–50 Hz) bands. Coherence in these frequency bands is believed to play a role in attention, memory, motor control, and plasticity (16, 18–20). As

Significance

Sensorimotor integration is important for the acquisition and performance of motor skills. Here, we show the emergence of neuroplastic changes in the interactions between the motor and somatosensory areas of the primate cortex during learning. Interareal coherence is frequency- and network-specific and exhibits a spatiotemporal organization. Time-sensitive sensorimotor integration and plasticity may rely on coherence of local and large-scale sensorimotor networks in order for cortical processes to operate at multiple temporal and spatial scales. Understanding cortico-cortical interactions may be important for developing therapies for sensorimotor disorders, such as those affecting feeding and speech that are commonly found in stroke and Parkinson's disease.

Author contributions: F.I.A.-M., C.F.R., B.J.S., and N.G.H. designed research; F.I.A.-M. performed research; C.F.R., K.T., B.J.S., and N.G.H. provided input to the analyses and write-up; F.I.A.-M. analyzed data; and F.I.A.-M. wrote the paper.

The authors declare no conflict of interest.

This article is a PNAS Direct Submission.

[1]To whom correspondence may be addressed. Email: fritziea@uchicago.edu or nicho@uchicago.edu.

This article contains supporting information online at www.pnas.org/lookup/suppl/doi:10.1073/pnas.1600788113/-/DCSupplemental.

NEUROSCIENCE

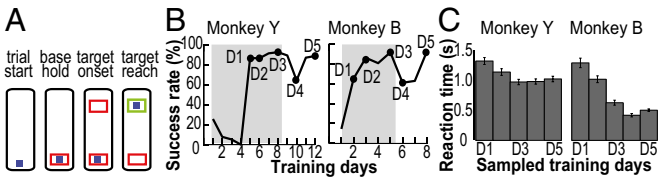

Fig. 1. Behavioral task and performance. (*A*) Diagram of the sequence of events in a trial of the tongue protrusion task. The blue square represents the force cursor, whereas the red and green boxes represent the base and force targets. (*B*) Success rates shown separately for each monkey. Dots mark the 5 d that were analyzed (i.e., sampled training days D1 to D5). Shaded area corresponds to training days when the required force level was 50 g. Required force level was increased to 80 g when success rates reached >75% for at least 3 consecutive days. (*C*) Reaction time shown as mean (±1 SEM error bars) across all trials for D1 to D5. *B* and *C* adapted from ref. 16.

the results for alpha/beta were similar to gamma, we only discuss the results in the gamma band here and show the results for alpha and beta bands in *Supporting Information*.

Frequency-Specific Modulation of Spike–Spike Coherence (MS) During Task Performance. Coherence between the spiking of MIo and SIo neurons (MS) at multiple frequencies was dynamically modulated; single neuronal pairs exhibited increases and decreases in coherence as well as firing-rate modulations relative to the onset of tongue-protrusive force (Fig. 2 *B* and *C*, and Fig. S1). Similar patterns were observed for the mean MS coherence across neuronal pairs with significant modulation of coherence (Fig. 2*D*, shuffle test, $P < 0.01$), consistent with the task modulation of theta coherence previously found within MIo and within SIo (16). Out of all of the possible combinations of paired signals ($n = 44{,}152$) from 10 datasets, the proportion of neuronal pairs that showed significant task modulation of MS coherence (i.e., "functional network") was highest in theta and was significantly lower in the higher frequency bands (Fig. S1*E*, McNemar test, $P < 0.01$). The larger theta network (i.e., highest proportion of paired neurons with significant coherence) exhibited the strongest coherence (i.e., highest mean peak coherence), whereas the sparser networks in the alpha/beta/gamma bands exhibited weaker coherence. This was observed for each monkey (Fig. 2*E*) and for data pooled across monkeys [Kruskal–Wallis peak by frequency, $x^2_{(3,20332)} = 10{,}683$, $P = 0$, post hoc, $P < 0.001$]. Differences in spectral power across frequencies cannot explain this result as the cross-spectrum is normalized by the autospectra. We also found frequency-specific differences in the time of peak MS coherence; pairs of MIo and SIo neurons exhibited a unimodal distribution of time of peak coherence in theta and a bimodal distribution in all other frequency bands [Fig. 2*F*, Kruskal–Wallis peak times by frequency, $x^2_{(3,20332)} = 122$, $P =$ 3e-26]. The mean time to peak theta coherence (0.03 s, SD = 0.07) occurred before and at force onset (note that coherence values were aligned to the right edge of the 0.5-s window). This suggests that theta coherence may play a role in generating the tongue-protrusive force. In contrast, the distribution of the times of peak gamma coherence was bimodal based on a two-component Gaussian mixture model having the lowest Akaike information criterion compared with models with one, three, or four components. The bimodal distribution of the peak times of gamma coherence was further confirmed by extending the time windows analyzed relative to force onset (Fig. 2*F*, *Inset*, and Fig. S2), indicating a suppression of gamma coherence at force onset. Peaks

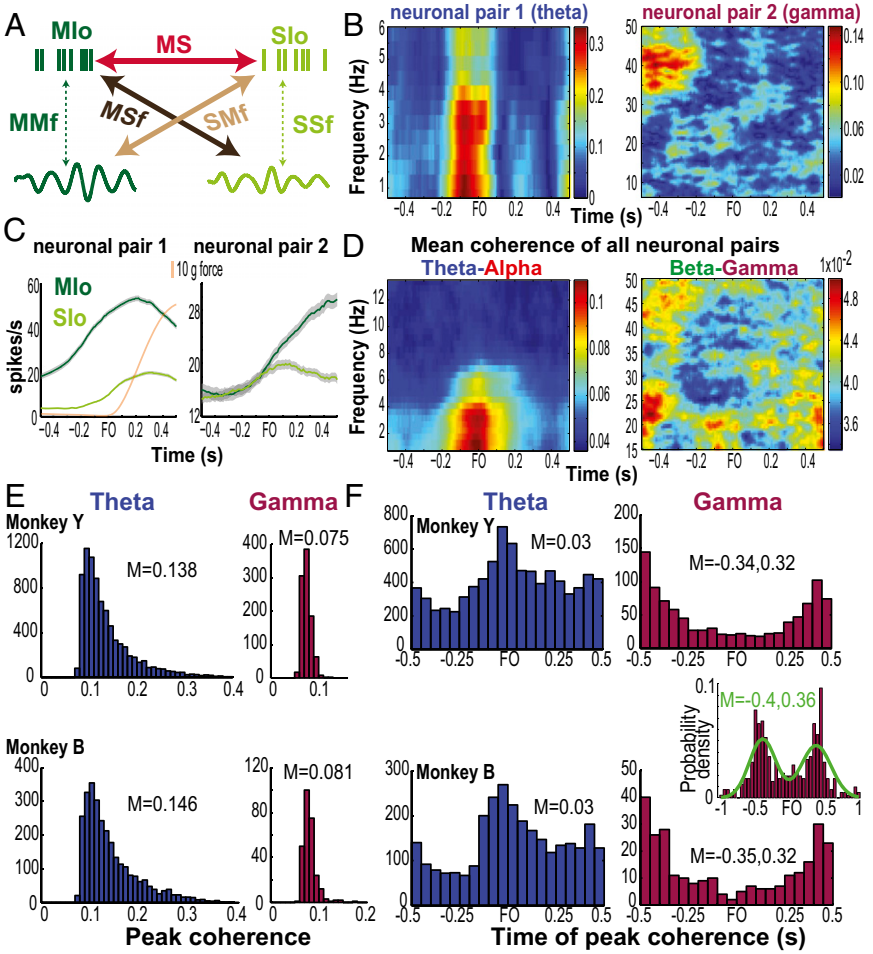

Fig. 2. Frequency-specific modulation of MS coherence between MIo and SIo neurons. (*A*) Schema of paired signals used in interareal coherence: paired spikes from MIo and SIo (MS), paired MIo spikes and SIo LFPs (MSf), and paired SIo spikes and MIo LFPs (SMf). We also analyzed intraareal coherence, i.e., paired spikes and LFPs within each area (MMf and SSf). (*B*) Coherogram of two pairs of neurons with significant MS coherence (color scale). Coherence is aligned to the right edge of the 0.5-s window, e.g., coherence at force onset (FO) corresponds to a 0.5-s window ending at FO. (*C*) Mean firing rates of MIo and SIo neurons whose coherent activity is shown in *B*. Rates were calculated using a 0.5-s sliding window with 0.01-s steps per trial then averaged across trials. Gray shades denote 1 SEM. Orange line denotes mean tongue-protrusive force of the first 100 trials of a training day. The force profile is averaged over a 0.5-s window. Timescales for rates and force are plotted to the right edge of 0.5-s window over which they were computed. (*D*) Mean coherence across all unique pairs of neurons (*SI Methods*) with significant coherence in one dataset, shown for the theta–alpha bands ($n = 75$ pairs) and beta–gamma bands ($n = 67$), respectively. (*E*) Histograms of peak coherence of all pairs with significant coherence in the theta and gamma bands. Shown for monkeys Y ($n_{theta} = 8{,}148$, $n_{gamma} = 967$) and B ($n_{theta} = 2{,}874$, $n_{gamma} = 271$) separately. Data pooled across D1 to D5. M, mean. (*F*) As in *E*, for time of peak coherence. (*Inset*) Histogram of time of peak gamma coherence ranging from –1.5 and 1 s relative to FO. Green line indicates Gaussian mixture model fit using two components. Data include only unique neuronal pairs with significant modulation of coherence, pooled across days and monkeys.

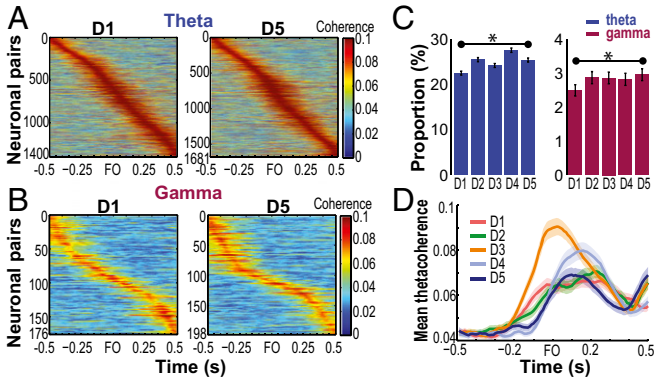

Fig. 3. Modulation of MS coherence by learning. (*A* and *B*) MS coherence of neuronal pairs with significant coherence in the theta and gamma bands, respectively, for D1 and D5 of monkey Y. Each plot shows changes in coherence of a neuronal pair (corresponding to a row in the *y* axis) relative to FO. Neuronal pairs are sorted according to the time of peak coherence relative to FO. (*C*) Day-to-day changes in the proportion of neuronal pairs with significant modulation of MS coherence. Data pooled across monkeys: in both theta and gamma bands, proportion increased from D1 (n_{theta} = 1,971/8,770, n_{gamma} = 219/8,770) to D5 (n_{theta} = 2,306/9,089, n_{gamma} = 269/9,089). *$P < 0.05$. Error bars indicate ±1 SEM (based on a binomial distribution assumption). (*D*) Day-to-day changes in MS theta coherence. Shown as mean (±1 SEM) coherence across pairs of stable neurons in monkey Y.

in gamma coherence [mean (M) = –0.35 s, 0.33 s (SD = 0.02) relative to force onset] occurred when monkeys were getting ready to apply the tongue-protrusive force or when monkeys were decreasing force production after being rewarded. On average, monkeys reached the force target at 0.15 s (SEM = 0.02) after force onset. Force offset typically occurred 0.5 s after force onset. The results of the coherence analyses in the theta band using a 0.5-s window were similar to the coherence results using a 1-s window (Fig. S3), and in the gamma band, the results using a 0.5-s window were similar to the results using a 0.3-s window.

In sum, task-modulated MS coherence differed between low- and high-frequency bands in terms of network size (i.e., the number of paired neurons with significant coherence in a specific band), peak time, and peak magnitude. Such dynamic modulation cannot be attributed to common task-related modulation nor to common inputs received by the neuronal pair because the shuffling procedure effectively estimates these coincident effects. A cross-validation approach (*SI Results* and Figs. S4 and S5) and performing the same analyses using only unique neuronal pairs further confirmed the dynamic modulation of coherence.

Changes in Spike–Spike Coherence (MS) with Learning. Fig. 3 *A* and *B* illustrates the coherent activity of the population of paired MIo–SIo neurons for D1 and D5 of monkey Y. Proportions of neuronal pairs with significant modulation of MS coherence changed during training from day to day. We tested statistical significance between D1 and D5 for each band and found $P < 0.05$ (Fig. 3*C*, binomial test). We also found day-to-day changes in peak and time of peak coherence in the theta band [Fig. 3*D* and Fig. S6, Kruskal–Wallis, peak by days: $x^2_{(4,11017)} = 53$, P = 7e-11; peak time by days: $x^2_{(4,11017)} = 32$, P = 2e-6] but not in the other frequency bands (Kruskal–Wallis, $P > 0.10$, peak/time of peak coherence by days separately for alpha/beta/gamma). We did not find any systematic changes in peak and time of peak coherence in relation to changes in tongue protrusion force, success rates, and reaction and movement times (Fig. S7, Pearson's correlation, $P > 0.10$). Furthermore, changes in firing rates cannot account for changes in MS coherence; no significant correlation was found between mean firing rates and mean MS coherence (Fig. S8, Pearson's correlation, $P > 0.10$). These indicate that coherence does not directly relate to the encoding of specific behavioral parameters and suggests a role of coherence in the spatiotemporal coordination of different functional networks that emerge or are reshaped during learning.

Network-Specific Modulation of Spike–Field Coherence. LFPs are considered to represent the aggregate subthreshold activity of neurons in a localized area near the recording electrode (21, 22), thereby providing information about the inputs to an area. A brief description of LFP properties in the orofacial sensorimotor cortex relevant to our analyses is presented in the *SI Results* and Figs. S9 and S10. Interareal spike–field coherence (MSf and SMf) also exhibited task modulation across multiple frequencies as illustrated for single pairs and for the population of paired signals (Fig. 4 *A* and *B*, and Fig. S11). The task modulation of MSf and SMf coherence was distinct from the modulation of LFP spectral power in MIo and SIo (Fig. S10). As was found in MS coherence, the spike–field coherent networks were large and strong in theta and were sparse and weak in alpha/beta/gamma [Fig. S12; McNemar test, $P < 0.01$; Kruskal–Wallis, peak by

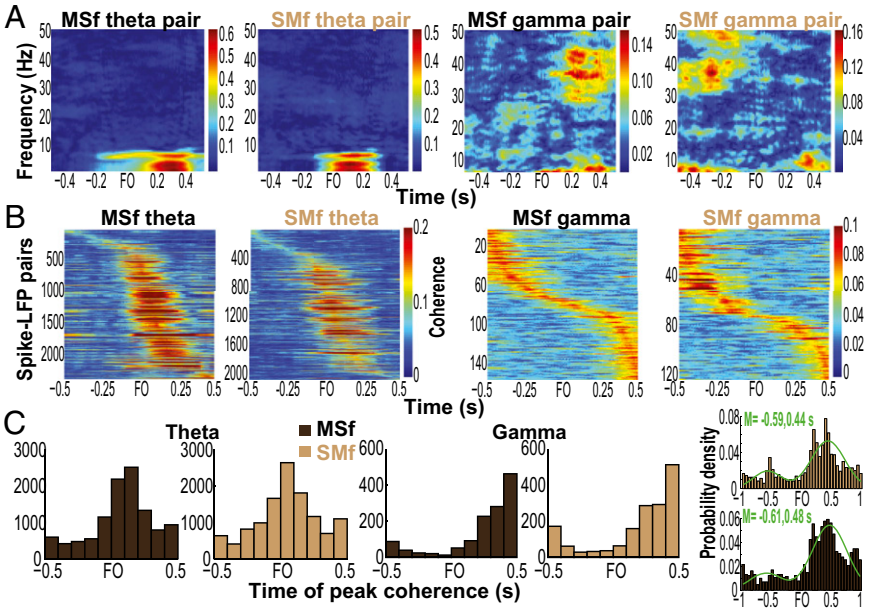

Fig. 4. Network-specific modulation of spike–field coherence. (*A*) Each coherogram shows spike–field coherence (MSf or SMf) of a single pair of signals as a function of frequency. (*B*) Theta and gamma spike–field coherence (MSf or SMf) of a population of pairs (*y* axis) from one dataset. Each row is a coherogram from a pair of signals and is the average over the theta (2–6 Hz) or gamma (30–50 Hz) band. Paired signals are sorted according to the time of peak coherence relative to FO. (*C*) Histograms of time of peak coherence for theta and gamma bands in MSf and SMf. Data pooled across training days and monkeys. (*Inset*) Histograms of time of peak gamma coherence (SMf and MSf) ranging from –1.5 and 1 s relative to FO. Green line indicates Gaussian mixture best model fit using two components. M, mean.

NEUROSCIENCE

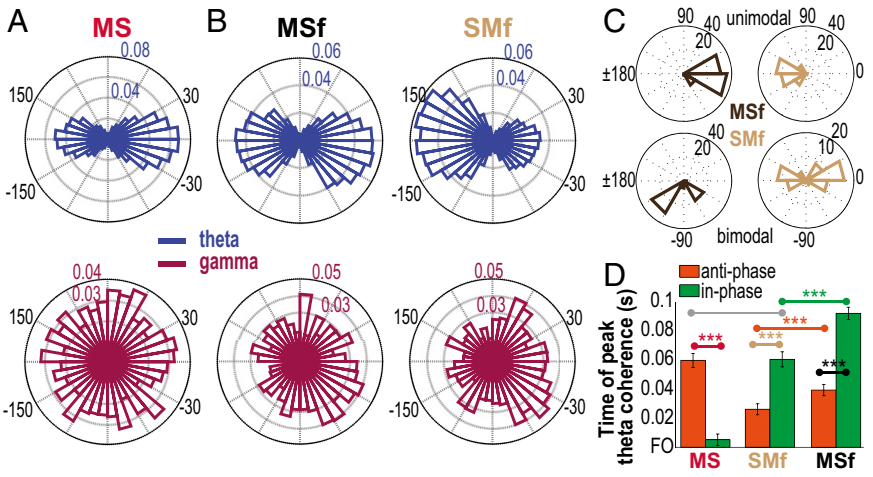

Fig. 5. Bimodal distribution of phase at peak coherence reveals subnetworks in theta. (*A*) Distributions of phase at peak coherence at 6 Hz (theta) and 40 Hz (gamma) for MS coherence. Data pooled across D1 to D5 of both monkeys and normalized by the total count in each frequency. (*B*) As in *A*, for MSf and SMf. (*C*) Four examples of theta Cϕ distribution of a single neuron with all LFP channels. MIo or SIo neurons in MSf or SMf, respectively, exhibited either a unimodal (top plots) or bimodal (bottom plots) Cϕ distribution in theta. (*D*) Mean (±1 SEM error bars) time of peak theta coherence relative to FO of in-phase and antiphase subnetworks of MS, SMf, and MSf. Paired comparisons denoted by connected dots whose colors correspond to specific networks. ***$P < 0.001$.

frequency, MSf: $x^2_{(3,17991)} = 3558$, $P = 0$; SMf: $x^2_{(3,19832)} = 2187$, $P = 0$, post hoc, $P < 0.01$]. Spike–field networks also exhibited preferred frequency bands; MSf coherence was stronger than SMf in theta, whereas SMf coherence was stronger than MSf in gamma [Kruskal–Wallis, peak by networks, theta: $x^2_{(3,46590)} = 3491$, $P = 0$; gamma: $x^2_{(3,6170)} = 70$, $P = 5e\text{-}15$; post hoc, $P < 0.001$]. Theoretic work has suggested that higher firing rates are correlated with stronger spike–field coherence (23). However, differences in firing rates of neurons cannot account for these results as no linear relations were found between firing rates of MIo or SIo neurons and the MSf/SMf coherence in either theta or gamma bands (Fig. S13). Temporal differences between theta and gamma also support the notion of frequency-specific roles of coherence in MIo and SIo. In theta MSf and SMf, the distributions of time of peak coherence were unimodal with peaks around force onset but the distributions were bimodal in gamma with peaks around ±0.35 s relative to force onset (Fig. 4*C* and Table S1).

Bimodal Distribution of Phase at Peak Coherence Reveals Subnetworks. The coherence analyses also measure the phase difference, $\phi_{xy}(t)$, between two signals x and y. Two signals are in-phase when $\phi_{xy}(t) = 0°$, or antiphase when $\phi_{xy}(t) = \pm 180°$. The phase at peak coherence (Cϕ) may provide important information on the temporal organization of the coherent signals. For MS coherence, the distribution of Cϕ was bimodal in theta (Fig. 5*A*, blue, Rayleigh test for bimodal distribution, $P < 0.00001$; circular mean: –2° and 178°) but uniform in gamma (Fig. 5*A*, fuchsia, Rayleigh test, $P > 0.10$). The bimodal distribution of theta Cϕ could not be explained by paired neurons that modulated their firing rates in phase (i.e., both neurons increased or decreased their firing rate concurrently) or out of phase (i.e., one increased its firing rate while the other decreased its firing rate) with each other relative to force generation (*SI Results*, Fig. S14). A similar bimodal distribution of theta Cϕ was observed in MSf and SMf (Fig. 5*B*, blue; Rayleigh test for bimodal distribution, $P < 0.00001$; circular mean: MSf: –4° and 176°; SMf: –6° and 174° at 6 Hz), but the gamma Cϕ distribution in MSf and SMf was unimodal (Fig. 5*B*, fuchsia, Rayleigh test for unimodal distribution, $P < 0.00001$; circular mean: MSf: –31°; SMf: –26° at 40 Hz). The bimodal distribution of theta Cϕ was also found in the intraareal coherence MMf and SSf (Rayleigh test for bimodal distribution, $P < 0.00001$). These results suggest two subnetworks of coherent signals, i.e., in-phase and antiphase. Thus, we examined the theta Cϕ distribution of each neuron with all other neurons in MS to see whether there were distinct subpopulations of neurons. We found that, in MS, a larger number of neurons exhibited a significant bimodal theta Cϕ distribution (Rayleigh test for bimodal distribution, $P < 0.05$; mean and SEM across D1–D5; Y: 61 ± 13%; B: 40 ± 9%) than unimodal distribution (Rayleigh test for unimodal distribution, $P < 0.05$; Y: 7 ± 2%; B: 4 ± 1%). We found the reverse for MSf and SMf; over 50% of single neurons in MIo and SIo exhibited a single preferred Cϕ relation with all theta oscillations in MSf and SMf, respectively (Fig. 5*C*, top plots; Rayleigh test for unimodal distribution, $P < 0.05$), whereas a smaller number of single

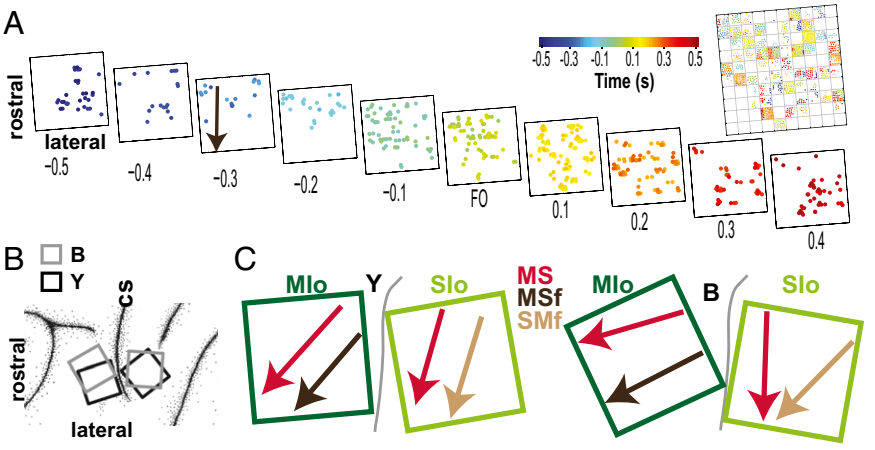

Fig. 6. Coherent activity follows a spatiotemporal pattern. (*A*) Square panels represent a map of the time of peak theta MSf coherence per position of each MIo neuron on the microelectrode array per 0.1-s block (monkey Y, D3). The orientation of the panel is matched to the array location on the cortex. The color of each dot represents the time of peak coherence relative to FO, and the positions of the dots have been jittered to show all individual MSf coherence values at each electrode. Arrow represents the direction of the linear relation between the time of peak coherence and the location of neurons on the microelectrode array. [*Inset* (*Top Right*)] All of the times of peak coherence on the 10 panels are plotted together in one panel to show the varied times of peak coherence (colored squares) for each electrode (area delineated by gray lines). (*B*) Location of the microelectrode arrays in MIo and SIo of monkeys Y and B. cs, central sulcus. (*C*) Summary of the mean direction of the progression of the time of peak coherence of the neurons in MIo and SIo for MS, MSf, and SMf. Shown for monkeys B and Y.

neurons showed two preferred Cϕ (Fig. 5*C*, bottom plots; Y: MSf, 17 ± 5%, SMf, 13 ± 3%; B: MSf, 21 ± 6%, SMf, 19 ± 5%). We verified that phase lags did not depend on specific LFP channels because Cϕ distributions of each LFP channel with all single units were also bimodal (0° and ± 180°). Last, we examined the temporal organization based on the Cϕ by comparing the time of peak coherence of paired signals whose Cϕ fell between –30° to 30° (i.e., the in-phase subnetwork) and between –150° to 150° (i.e., the antiphase subnetwork). In MS, time of peak coherence of the in-phase neurons was significantly earlier than that of the antiphase neurons (Fig. 5*D*, red; Mann–Whitney, $P < 0.001$). However, in both SMf and MSf, the antiphase subnetwork had significantly earlier time of peak coherence than the in-phase subnetwork (Fig. 5*D*, brown and black; $P < 0.001$). Time of peak coherence of both in-phase and antiphase subnetworks in SMf were significantly earlier than in MSf (Fig. 5*D*, green and orange; $P < 0.001$). These results indicate temporal differences based on Cϕ and the network: in-phase MS ($n = 4{,}046$) → antiphase SMf ($n = 3{,}842$) → antiphase MSf ($n = 2{,}873$) → antiphase MS ($n = 2{,}895$) and in-phase SMf ($n = 2{,}229$) → in-phase MSf ($n = 3{,}217$).

Coherent Activity Follows a Spatiotemporal Pattern. Fig. 3 *A* and *B* shows that coherent neuronal pairs do not reach their peak activity all at the same time. Does the spatial location of coherent neurons influence the timing and the magnitude of their peak coherence? We tested this in MS, MSf, and SMf for both theta and gamma coherence but only found significant results in theta (*SI Results*, Table S2, and Fig. S15). Fig. 6*A* maps the mediolateral progression of the time of peak theta MSf coherence on the MIo array from D3 of monkey Y; the spatial gradient was apparent from 0.3 s before force onset when MIo neurons located medially exhibited the earliest peak MSf coherence. At 0.4 s after force onset, MIo neurons that exhibited peak coherence were mostly at the lateral border. The mean (across training days) spatial gradient for time of peak theta coherence for MIo neurons in MS and MSf was initiated close to the central sulcus and progressed in the rostrolateral direction (Fig. 6 *B* and *C*, MIo array). This may be related to our previous finding that MIo neurons whose spiking activity led the tongue-protrusive force were located closer to the central sulcus than neurons whose spiking activity lagged the force (16). For SIo neurons in MS and SMf, the mean spatial gradient for time of peak theta coherence was from medial to lateral (Fig. 6*C*, SIo array). Because opening of the lips preceded tongue protrusion, the spatial gradient of the time of peak coherence may relate to the order in which sensory information was received from the lips and the tongue. Indeed, mechanoreceptive fields (RFs) of the lips are located at the medial border of SIo and RFs of the tongue at the lateral border of SIo (24). For the LFP component of MSf and SMf, time of peak coherence progressed medially and toward the central sulcus for MSf and medially for SMf (Fig. S14*A*, dashed arrows). The results suggest a spatiotemporal organization of coherence based on the temporal relation of MIo neurons' spiking to tongue force and on the spatial features of MIo and SIo neurons' RFs.

Discussion

To our knowledge, this study provides the first documentation of the emergence of neuroplastic changes in the coherence between motor and somatosensory areas of the primate cortex during sensorimotor learning. Interareal coherence was frequency- and network-specific and exhibited a spatiotemporal organization. Such interactions may imply communication between sensory and motor cortical areas for integrating new sensory and motor events and for forming and retrieving memories during learning.

Coherent Networks Involve Multiple Frequencies. The simultaneous presence of cortical rhythms in multiple frequencies in the arm sensorimotor cortex has been reported (25, 26), but (to our knowledge) this is the first documentation of frequency-specific coherent activity in the orofacial sensorimotor cortex. Larger and stronger sensorimotor networks occurred in theta, whereas sparser and weaker networks occurred in alpha/beta/gamma, consistent with the general feature of cortical rhythms that slow oscillations engage larger networks whereas fast oscillations engage more localized networks (27). Synchronous activity of local- and large-scale networks may be organized through multiple frequency bands for different cortical processes to operate at multiple temporal and spatial scales. Specifically, different functional demands at different phases of the task may require interareal coherence at different frequencies. Previous studies in the arm sensorimotor cortex suggest that theta synchrony is organized according to movement phases (28, 29). Thus, the high theta coherence at force onset may relate to the generation of tongue-protrusive force. In contrast, the high gamma coherence before and after force onset may relate to other processes such as sensory gating (30, 31), attention (18), and memory encoding/retrieval in association with theta coherence (32).

Reciprocal Interaction Between MIo and SIo. The observed interactions between MIo and SIo may be explained by a common source of modulatory activity, such as from the thalamus and not due to direct cortico-cortical communication. There are abundant projections from thalamus to MIo and SIo (11, 33), and thalamic neurons have been found to oscillate at 6, 10, and 40 Hz and thus have the potential to generate an oscillatory drive to the cortex in these frequencies (32, 34, 35). However, oscillations may be initiated in the cortex and propagated to the thalamus, which then sends oscillations back to the cortex, thus increasing the cortico-thalamo-cortical resonance (36). This is in agreement with findings in rats, which have spike-and-wave discharges originating from SIo, and then propagating to the thalamus (37). Alternatively, our results may instead represent a direct interaction between MIo and SIo. The dense anatomical connections between MIo and SIo provide a substrate for coherent firing of neurons that may underlie the formation of neuronal assemblies (2, 38, 39). Thus, the increased proportion of coherent neurons may represent the new coupling of a motor output to specific sensory inputs as learning unfolds. Our results also suggest that this process involves reciprocal interactions; MIo modulates sensory processing in SIo (40, 41) and SIo transmits afferent information to MIo critical for successful task performance (5, 6, 42, 43). Because both MIo and SIo have bilateral orofacial representations, cross-hemisphere interactions in the orofacial sensorimotor area may share some properties of the intercortical coherence observed here.

Coherence Phase Reveals Temporal Organization of Subnetworks. To our knowledge, this study is the first to report a bimodal distribution of phase at peak theta coherence in the sensorimotor cortex, i.e., in-phase (zero lag) and antiphase (near 180° lag). Zero-lag coherence has been suggested to result from either common input, reciprocal interaction, or a combination of both (44), whereas non–zero-lag coherence in gamma has been suggested to reflect interareal conduction delays in unidirectional interactions (45–47). Antiphase synchronization (15–30 Hz) between spikes in the parietal reach region and LFPs in the dorsal premotor cortex has been implicated in down-modulation of communication to selectively prevent transmission of movement-related information (48). Likewise, bimodal distributions of relative phases (0° and 180°) between LFPs (8–25 Hz) in the prefrontal and posterior parietal cortical areas has been suggested to represent specific patterns of coupling among neurons in these areas (49). Given that conduction delays within an area and even across areas are much smaller than the half period of a theta cycle, the antiphase relations in theta coherence found here are likely not due to conduction delays but may represent different populations of MIo neurons whose activity either leads or lags the force generation (16, 49) or a down-modulation of communication between MIo and SIo to prevent transmission of irrelevant sensory or movement-related information (48). The results further refine the understanding of the temporal sequence of coherent activity between MIo and SIo and suggest that cortico-cortical

coherence may use phase to organize the activity of neuronal assemblies at different timescales or for segregating feedforward and feedback influences so that orofacial sensorimotor behaviors using different muscles and motor patterns are appropriately coordinated during learning.

Methods

Subjects. All experiments were performed in two adult male rhesus macaques (*Macaca mulatta*), B (10 kg) and Y (12 kg). All protocols were approved by the University of Chicago Animal Care and Use Committee and complied with the National Institutes of Health *Guide for the Care and Use of Laboratory Animals* (50).

Behavioral Task. We used a long-term learning paradigm wherein the subjects were exposed to the same behavioral task parameters over days until subjects achieve a success rate >75% consistently for 3 d (16). Monkeys were trained to protrude the tongue onto a force transducer and apply isometric force at the level cued by target positions. Fig. 1*A* illustrates the sequence of events in a trial. Detailed description of the task can be found in *SI Methods*. The behavioral program was written using Spike2 software (Cambridge Electronic Design). Force transducer (Revere Transducers; mode 462-D3-2-10P1R) signals and the behavioral event logs and time stamps were recorded at 2 kHz and stored using a Power 1401 data acquisition system (Cambridge Electronic Design). User-designed pulse signals were generated to mark behavioral events and were sent to the neural data acquisition systems for off-line synchronization of time stamps across the different data acquisition systems.

Further details are available in *SI Methods*.

ACKNOWLEDGMENTS. We thank Dr. Jason Lee, Kevin Brown, and Dr. Kate Murray for assistance with the experiments; Prof. Yali Amit for help with the statistical analyses; Dr. Aaron Suminski and Matt Best for helpful discussions; and the veterinary staff of the University of Chicago for animal care. This work was supported by CIHR Grant MOP-4918, NIH Grant R01 DE023816, and the University of Chicago Research Computing Center.

1. Singer W, Gray CM (1995) Visual feature integration and the temporal correlation hypothesis. *Annu Rev Neurosci* 18:555–586.
2. Fries P (2005) A mechanism for cognitive dynamics: Neuronal communication through neuronal coherence. *Trends Cogn Sci* 9(10):474–480.
3. DeCoteau WE, et al. (2007) Learning-related coordination of striatal and hippocampal theta rhythms during acquisition of a procedural maze task. *Proc Natl Acad Sci USA* 104(13):5644–5649.
4. Thorn CA, Graybiel AM (2014) Differential entrainment and learning-related dynamics of spike and local field potential activity in the sensorimotor and associative striatum. *J Neurosci* 34(8):2845–2859.
5. Brovelli A, et al. (2004) Beta oscillations in a large-scale sensorimotor cortical network: Directional influences revealed by Granger causality. *Proc Natl Acad Sci USA* 101(26): 9849–9854.
6. Witham CL, Wang M, Baker SN (2010) Corticomuscular coherence between motor cortex, somatosensory areas and forearm muscles in the monkey. *Front Syst Neurosci* 4:38.
7. Murthy VN, Fetz EE (1992) Coherent 25- to 35-Hz oscillations in the sensorimotor cortex of awake behaving monkeys. *Proc Natl Acad Sci USA* 89(12):5670–5674.
8. Sessle BJ (2006) Mechanisms of oral somatosensory and motor functions and their clinical correlates. *J Oral Rehabil* 33(4):243–261.
9. Avivi-Arber L, Martin R, Lee JC, Sessle BJ (2011) Face sensorimotor cortex and its neuroplasticity related to orofacial sensorimotor functions. *Arch Oral Biol* 56(12):1440–1465.
10. Huang CS, Hiraba H, Sessle BJ (1989) Input-output relationships of the primary face motor cortex in the monkey (*Macaca fascicularis*). *J Neurophysiol* 61(2):350–362.
11. Hatanaka N, Tokuno H, Nambu A, Inoue T, Takada M (2005) Input-output organization of jaw movement-related areas in monkey frontal cortex. *J Comp Neurol* 492(4):401–425.
12. Kuypers HG (1958) Some projections from the peri-central cortex to the pons and lower brain stem in monkey and chimpanzee. *J Comp Neurol* 110(2):221–255.
13. Lin LD, Sessle BJ (1994) Functional properties of single neurons in the primate face primary somatosensory cortex. III. Modulation of responses to peripheral stimuli during trained orofacial motor behaviors. *J Neurophysiol* 71(6):2401–2413.
14. Murray GM, Sessle BJ (1992) Functional properties of single neurons in the face primary motor cortex of the primate. I. Input and output features of tongue motor cortex. *J Neurophysiol* 67(3):747–758.
15. Arce FI, Lee JC, Ross CF, Sessle BJ, Hatsopoulos NG (2013) Directional information from neuronal ensembles in the primate orofacial sensorimotor cortex. *J Neurophysiol* 110(6):1357–1369.
16. Arce-McShane FI, Hatsopoulos NG, Lee J-C, Ross CF, Sessle BJ (2014) Modulation dynamics in the orofacial sensorimotor cortex during motor skill acquisition. *J Neurosci* 34(17):5985–5997.
17. Boudreau SA, et al. (2013) Features of cortical neuroplasticity associated with multidirectional novel motor skill training: A TMS mapping study. *Exp Brain Res* 225(4):513–526.
18. Fell J, Axmacher N (2011) The role of phase synchronization in memory processes. *Nat Rev Neurosci* 12(2):105–118.
19. Siegel M, Donner TH, Engel AK (2012) Spectral fingerprints of large-scale neuronal interactions. *Nat Rev Neurosci* 13(2):121–134.
20. Menzer DL, Rao NG, Bondy A, Truccolo W, Donoghue JP (2014) Population interactions between parietal and primary motor cortices during reach. *J Neurophysiol* 112(11):2959–2984.
21. Mitzdorf U (1985) Current source-density method and application in cat cerebral cortex: Investigation of evoked potentials and EEG phenomena. *Physiol Rev* 65(1):37–100.
22. Katzner S, et al. (2009) Local origin of field potentials in visual cortex. *Neuron* 61(1):35–41.
23. Lepage KQ, Kramer MA, Eden UT (2011) The dependence of spike field coherence on expected intensity. *Neural Comput* 23(9):2209–2241.
24. Huang CS, Hiraba H, Murray GM, Sessle BJ (1989) Topographical distribution and functional properties of cortically induced rhythmical jaw movements in the monkey (*Macaca fascicularis*). *J Neurophysiol* 61(3):635–650.
25. Popivanov D, Mineva A, Krekule I (1999) EEG patterns in theta and gamma frequency range and their probable relation to human voluntary movement organization. *Neurosci Lett* 267(1):5–8.
26. Jackson A, Spinks RL, Freeman TCB, Wolpert DM, Lemon RN (2002) Rhythm generation in monkey motor cortex explored using pyramidal tract stimulation. *J Physiol* 541(Pt 3):685–699.
27. Buzsáki G, Draguhn A (2004) Neuronal oscillations in cortical networks. *Science* 304(5679):1926–1929.
28. Feige B, Aertsen A, Kristeva-Feige R (2000) Dynamic synchronization between multiple cortical motor areas and muscle activity in phasic voluntary movements. *J Neurophysiol* 84(5):2622–2629.
29. Ohara S, et al. (2001) Increased synchronization of cortical oscillatory activities between human supplementary motor and primary sensorimotor areas during voluntary movements. *J Neurosci* 21(23):9377–9386.
30. Cardin JA, et al. (2009) Driving fast-spiking cells induces gamma rhythm and controls sensory responses. *Nature* 459(7247):663–667.
31. Engel AK, Fries P, König P, Brecht M, Singer W (1999) Temporal binding, binocular rivalry, and consciousness. *Conscious Cogn* 8(2):128–151.
32. Ketz NA, Jensen O, O'Reilly RC (2015) Thalamic pathways underlying prefrontal cortex-medial temporal lobe oscillatory interactions. *Trends Neurosci* 38(1):3–12.
33. Cerkevich CM, Qi H-X, Kaas JH (2013) Thalamic input to representations of the teeth, tongue, and face in somatosensory area 3b of macaque monkeys. *J Comp Neurol* 521(17):3954–3971.
34. Steriade M, Gloor P, Llinás RR, Lopes de Silva FH, Mesulam MM (1990) Report of IFCN Committee on Basic Mechanisms. Basic mechanisms of cerebral rhythmic activities. *Electroencephalogr Clin Neurophysiol* 76(6):481–508.
35. Poulet JFA, Fernandez LMJ, Crochet S, Petersen CCH (2012) Thalamic control of cortical states. *Nat Neurosci* 15(3):370–372.
36. Llinás RR (2014) Intrinsic electrical properties of mammalian neurons and CNS function: A historical perspective. *Front Cell Neurosci* 8(November):320.
37. Polack P-O, Mahon S, Chavez M, Charpier S (2009) Inactivation of the somatosensory cortex prevents paroxysmal oscillations in cortical and related thalamic neurons in a genetic model of absence epilepsy. *Cereb Cortex* 19(9):2078–2091.
38. Gerstein GL, Bedenbaugh P, Aertsen MH (1989) Neuronal assemblies. *IEEE Trans Biomed Eng* 36(1):4–14.
39. Hayashi-Takagi A, et al. (2015) Labelling and optical erasure of synaptic memory traces in the motor cortex. *Nature* 525(7569):333–338.
40. Zagha E, Casale AE, Sachdev RNS, McGinley MJ, McCormick DA (2013) Motor cortex feedback influences sensory processing by modulating network state. *Neuron* 79(3):567–578.
41. Petreanu L, et al. (2012) Activity in motor-sensory projections reveals distributed coding in somatosensation. *Nature* 489(7415):299–303.
42. Lee J-C, Sood M, Sessle BJ (2011) The effects of orofacial sensory loss on tongue-protrusion task performance in monkeys. *Soc Neurosci Abstr* 37:809.13.
43. Lin LD, Murray GM, Sessle BJ (1993) The effect of bilateral cold block of the primate face primary somatosensory cortex on the performance of trained tongue-protrusion task and biting tasks. *J Neurophysiol* 70(3):985–996.
44. Rajagovindan R, Ding M (2008) Decomposing neural synchrony: Toward an explanation for near-zero phase-lag in cortical oscillatory networks. *PLoS One* 3(11):e3649.
45. Bastos AM, Vezoli J, Fries P (2015) Communication through coherence with inter-areal delays. *Curr Opin Neurobiol* 31:173–180.
46. Bosman CA, et al. (2012) Attentional stimulus selection through selective synchronization between monkey visual areas. *Neuron* 75(5):875–888.
47. Grothe I, Neitzel SD, Mandon S, Kreiter AK (2012) Switching neuronal inputs by differential modulations of gamma-band phase-coherence. *J Neurosci* 32(46):16172–16180.
48. Stetson C, Andersen RA (2014) The parietal reach region selectively anti-synchronizes with dorsal premotor cortex during planning. *J Neurosci* 34(36):11948–11958.
49. Dotson NM, Salazar RF, Gray CM (2014) Frontoparietal correlation dynamics reveal interplay between integration and segregation during visual working memory. *J Neurosci* 34(41):13600–13613.
50. National Research Council (2011) *Guide for the Care and Use of Laboratory Animals* (National Academies Press, Washington, DC), 8th Ed.
51. Mitra PP, Pesaran B (1999) Analysis of dynamic brain imaging data. *Biophys J* 76(2):691–708.
52. Bokil HS, Pesaran B, Andersen RA, Mitra PP (2006) A method for detection and classification of events in neural activity. *IEEE Trans Biomed Eng* 53(8):1678–1687.
53. Berens P (2009) CircStat: A MATLAB toolbox for circular statistics. *J Stat Softw* 31(10):1–21.
54. Le Van Quyen M, et al. (2001) Comparison of Hilbert transform and wavelet methods for the analysis of neuronal synchrony. *J Neurosci Methods* 111(2):83–98.
55. Rubino D, Robbins KA, Hatsopoulos NG (2006) Propagating waves mediate information transfer in the motor cortex. *Nat Neurosci* 9(12):1549–1557.
56. Toda T, Taoka M (2002) Hierarchical somesthetic processing of tongue inputs in the postcentral somatosensory cortex of conscious macaque monkeys. *Exp Brain Res* 147(2):243–251.